HHS Public Access

Author manuscript

J Neuroimaging. Author manuscript; available in PMC 2023 July 01.

Published in final edited form as:

J Neuroimaging. 2022 July ; 32(4): 697–709. doi:10.1111/jon.12990.

Brain oxygen extraction and neural tissue susceptibility are associated with cognitive impairment in older individuals

Gloria C Chiang[1,*], **Junghun Cho**[2,*], **Jonathan Dyke**[3], **Hang Zhang**[4], **Qihao Zhang**[4], **Michael Tokov**[5], **Thanh Nguyen**[2], **Ilhami Kovanlikaya**[1], **Michael Amoashiy**[6], **Mony de Leon**[7], **Yi Wang**[2]

[1]Department of Radiology, Division of Neuroradiology, Weill Cornell Medicine, NewYork-Presbyterian Hospital, 525 East 68th Street, Starr Pavilion, Box 141, New York, NY 10065;

[2]MRI Research Institute, Department of Radiology, Weill Cornell Medicine, New York, NY

[3]Citigroup Biomedical Imaging Center, Weill Cornell Medicine, New York, NY

[4]Department of Biomedical Engineering, Cornell University, Ithaca, NY

[5]New York Institute of Technology College of Osteopathic Medicine, Glen Head, NY

[6]Department of Neurology, Weill Cornell Medicine, New York, NY

[7]Brain Health Imaging Institute, Department of Radiology, Weill Cornell Medicine, New York, NY

Abstract

Background and Purpose: We investigated the effects of aging, white matter hyperintensities (WMH), and cognitive impairment on brain iron levels and cerebral oxygen metabolism, known to be altered in Alzheimer's disease (AD), using quantitative susceptibility mapping and MR-based cerebral oxygen extraction fraction (OEF).

Methods: In 100 individuals over the age of 50 (68/32 cognitively impaired/intact), OEF and neural tissue susceptibility (χ_n) were computed retrospectively from MRI multi-echo gradient echo data, obtained on a 3 Tesla MRI scanner. The effects of age and WMH on OEF and χ_n were assessed within groups, and OEF and χ_n were assessed between groups, using multivariate regression analyses.

Results: Cognitively impaired subjects were found to have 19% higher OEF and 34% higher χ_n than cognitively intact subjects in the cortical gray matter and several frontal, temporal, and parietal regions ($p < 0.05$). Increased WMH burden was significantly associated with decreased OEF in the cognitively impaired, but not in the cognitively intact. Older age had a stronger association with decreased OEF in the cognitively intact group. Both older age and increased WMH burden were significantly associated with increased χ_n in temporoparietal regions in the cognitively impaired.

Corresponding author: Gloria C. Chiang, M.D., Department of Radiology, Division of Neuroradiology, Weill Cornell Medical College, NewYork-Presbyterian Hospital, 525 East 68th Street, Starr Pavilion, Box 141, New York, NY 10065, Phone: 212-746-2616, Fax: 212-746-8597, gcc9004@med.cornell.edu.

*Drs. Chiang and Cho contributed equally to this manuscript

Conclusions: Higher brain OEF and χ_n in cognitively impaired older individuals may reflect altered oxygen metabolism and iron in areas with underlying AD pathology. Both age and WMH have associations with OEF and χ_n but are modified by the presence of cognitive impairment.

Keywords

oxygen extraction; iron imaging; tissue susceptibility; cognitive impairment

Introduction

Cognitive impairment is widely prevalent among older individuals, affecting a reported twenty percent of adults over the age of 50.[1] Alzheimer's disease (AD) remains the most common cause of cognitive impairment among older adults, but definitive diagnosis requires the identification of beta-amyloid plaques and neurofibrillary tangles postmortem. Although advances in PET, cerebrospinal fluid, and plasma biomarkers provide opportunities to diagnose AD antemortem, these techniques are not yet reimbursed, so current clinical management typically relies on MRI and cognitive assessments. Initial workup of individuals with cognitive impairment therefore commonly includes MR imaging to exclude potentially reversible causes of dementia, even though these are found in fewer than ten percent of cases.[2]

Recent studies have shown that individuals with AD and mild cognitive impairment (MCI) have higher levels of brain iron compared to normal controls,[3–8] and iron levels can predict subsequent cognitive decline in amyloid-positive individuals.[3] Preclinical and postmortem studies have reported that iron colocalizes with beta-amyloid plaques[9–11] and is found within activated microglia associated with these plaques.[12,13] Higher iron levels in brain regions may therefore serve as a proxy for AD pathology. Quantitative susceptibility mapping (QSM),[14] a novel MRI technique that deconvolves the magnetic field measured in MRI to study tissue magnetism, is ideally suited for noninvasive quantification of strongly paramagnetic iron.[15–19] QSM has been validated by pathological correlation studies[20,21] and has been shown to be highly reproducible, even when performed at different sites, on different vendor platforms, and across field strengths.[22,23]

In addition to assessing tissue iron levels, QSM can be combined with a quantitative blood oxygen level-dependent magnitude (qBOLD) technique (QSM+qBOLD or QQ) to assess the oxygen extraction fraction (OEF).[24–28] The OEF is a physiologic marker that reflects the percentage of oxygen extracted from the arterial supply of the brain, which is associated with brain oxygen utilization and metabolism. MR-based OEF mapping has shown high agreement with OEF mapping using ^{15}O-PET[27,29] and is more easily implemented, since it utilizes a routinely available MR sequence without injection of tracers. Clinical feasibility of QQ has been shown in the settings of ischemic stroke[30,31] and multiple sclerosis.[32] As QQ further divides voxel-wise susceptibility into the effect of deoxyheme iron in a cylindrical micron-scale venule (OEF effect) and that of neural tissue susceptibility (χ_n) derived from diffuse nanoscale ferritin iron in tissue,[24] it can provide a comprehensive picture of both tissue oxygenation and iron.

Using QQ technique, we sought to investigate regional differences in brain iron and oxygen extraction in clinical cohorts of cognitively impaired and intact older individuals. Since older age[33] and white matter hyperintensities (WMH)[34] are strong predictors of cognitive impairment and dementia, we also investigated the effects of these variables on OEF and χ_n in the brain.

Methods:

Subjects and MR Image Acquisition

This study was approved by the Weill Cornell Medicine Institutional Review Board and was compliant with the Health Insurance Portability and Accountability Act; written informed consent was waived due to the retrospective nature of this study.

Sixty-eight cognitively impaired patients who were referred for an MRI of the brain between 2017 and 2020 were included in this analysis. These patients were evaluated by a neurologist and clinically suspected to have AD based on exclusion of alternative etiologies of dementia by neurological examination, neuropsychological assessment, laboratory data, and MRI. To confirm probable AD, fifty patients (74%) underwent an FDG-PET scan, which demonstrated a temporoparietal pattern of hypometabolism, with regional standardized uptake values measuring more than two standard deviations below normal, as compared to a normative database of individuals of a similar age (syngo.via software, Siemens Healthineers). Of these fifty, ten had abnormal cognitive scores on the Montreal Cognitive Assessment (MoCA),[35] nine on the Mini-Mental State Examination (MMSE),[36] fifteen on the Short Test of Mental Status (STMS),[37] and seven on a combination of verbal and visual memory tests; cognitive scores were not available in the medical record for the remaining nine, although one had a positive amyloid PET scan and two were noted to be too impaired to continue cognitive assessment. Five (7%) of the 68 cognitively impaired patients had cerebrospinal fluid (CSF) biomarkers consistent with AD; of these, three patients had abnormal MoCA scores, 1 had an abnormal MMSE score, and one had abnormal scores on both the MoCA and MMSE. One (1%) of the 68 impaired patients had a positive amyloid PET scan, as well as abnormal scores on both the MoCA and MMSE. Twelve (18%) of the 68 impaired patients had an MRI without FDG or amyloid PET; seven of these had abnormal MoCA scores, two had abnormal MMSE scores, 1 had an abnormal STMS score, and two had abnormal scores on multiple verbal and visual memory tests.

Thirty-two age-matched individuals who presented with headaches during the same time period and were presumed to have no history of cognitive symptoms were included as cognitively intact controls. Review of medical records also confirmed the absence of exclusion criteria including other neurological and systemic disorders that could affect the brain, including traumatic brain injury, territorial infarcts, epilepsy, cancer, hydrocephalus, history of birth injury, major depression and other psychiatric disorders, use of illicit substances, chronic kidney disease, and liver disease.

All patients underwent MR imaging on a 3 Tesla scanner (Skyra, Biograph mMR, Siemens Healthcare; Discovery 750w, Signa HDxt, GE Healthcare, Milwaukee, Wisconsin), which included a 3D T1-weighted sequence reconstructed at 1 mm slice thickness [Repetition

time (TR)/ Echo time (TE) 9/3 milliseconds with a flip angle of 15 degrees or TR/TE 600/11 milliseconds with a flip angle of 120 degrees], a 3D T2 fluid-attenuated inversion recovery (FLAIR) sequence reconstructed at 1 mm slice thickness (TR/TE 6300–8500/394–446 milliseconds, flip angle 120 degrees), and a 3D T2*-weighted multiecho gradient echo (mGRE) sequence (TR 49 milliseconds, $TE_1/\Delta TE/TE_{10}$ 6.7/4.1/43.2 milliseconds flip angle 15 degrees, voxel size $0.72\times0.72\times3$ mm^3). The mGRE sequence was acquired with flow compensation in the x and z directions, but not the y direction.

Image analysis

QSM was reconstructed by estimating the total field via a nonlinear fit of mGRE,[38] calculating the local field by the Projection onto Dipole Fields (PDF) method,[39] and computing susceptibility with the Morphology Enabled Dipole Inversion with automatic uniform CSF zero reference (MEDI+0) algorithm.[14,18,40,41] Our standard QSM processing excludes voxels that are 5mm from the outside boundary of the brain to minimize background field contamination into the QSM/OEF maps, typically from calvarium. In addition, voxels with an R2*>100 Hz or <2.5 Hz are excluded because these are mainly cerebrospinal fluid.

OEF and χ_n maps were estimated from QSM and mGRE magnitude using the QQ algorithm.[24,25,27] QQ combines two biophysics models of mGRE data: 1) a QSM processing of phase data to distinguish the susceptibility contribution of venous blood from that of neural tissue on a voxel level,[42–44] and 2) qBOLD modeling of the mGRE magnitude signal decay by the intravoxel magnetic field variation caused by the susceptibility difference between cylindrical venous blood and surrounding tissue.[45–47] For robust OEF estimation against measurement noise, the inverse condition of the QQ model was improved using similar OEF for the same tissue composition voxels with similar mGRE signal evolution[25] based on tissue segmentation into gray matter/white matter/CSF subclusters on T1-weighted image using FSL FAST algorithm,[48] and using sparsity in space and time,[27] OEF was reported as a decimal from 0 to 1 (unitless) and the unit of χ_n was parts per billion (ppb).

3D T1-weighted sequences were co-registered to the QSM maps to obtain global measures of tissue susceptibility and OEF, including cortical gray and white matter. In addition, Freesurfer[49] was used to segment the brain regions on the 3D T1-weighted images, and the region labels were then applied to the QSM maps. Bilateral regions were averaged. A priori, 20 brain regions that have previously been shown to be affected by AD and/or iron abnormalities were included in the analyses.[4,50,51] Specifically, we focused on temporal and parietal lobe regions that are commonly considered “AD signature” regions due to involvement by AD pathology, including the hippocampus, amygdala, superior, middle, and inferior temporal gyri, fusiform gyrus, posterior cingulate, isthmus cingulate, precuneus, superior and inferior parietal lobes, and supramarginal gyrus.[4,50,52] In addition, we included the basal ganglia and frontal lobe regions, including the superior, caudal middle, and rostral middle frontal gyri, since these regions have been reported to show abnormal iron deposition by QSM and amyloid deposition on PET.[4,51]

WMH lesions were segmented using a deep-learning approach with a convolutional neural network.[53] 3D T2 FLAIR sequences were registered to the QSM maps. These white matter

lesion masks were then manually edited. We used the volume fraction of WMH relative to whole brain as the measure of WMH burden in the analyses.

Statistical Analysis

All statistical analyses were programmed in STATA version 16 (StataCorp, College Station, TX). Comparisons of baseline variables among groups were performed using the Wilcoxon rank-sum test and Fisher exact test, depending on the type and distribution of the variables.

To assess the relationship between age and OEF or χ_n, we used ordinary least squares regression analyses, with OEF or χ_n, by region, as the outcome variable and age as the predictor variable. To assess the relationship between WMH and OEF or χ_n, we used ordinary least squares regression analyses, with OEF or χ_n, by region, as the outcome variable and WMH as the predictor variable. These analyses were performed in both groups.

To assess differences in OEF and χ_n between the cognitively impaired and cognitively intact groups, we used multivariate regression analysis. OEF or χ_n was used as the outcome variable, by region, and presence of cognitive impairment was included as the predictor variable. Age and WMH burden were included as covariates. A p-value of less than 0.05 was considered statistically significant. To adjust for multiple comparisons, the Benjamini-Hochberg method was used to obtain adjusted p-values.[54]

Results:

Subject characteristics are presented in Table 1. There were no significant group differences in age or sex distribution, although the cognitively impaired had a higher WMH burden.

Age showed associations with oxygen extraction in the cognitively intact group

In the cognitively intact group, individuals below the median age had a mean whole brain OEF of 0.26 ± 0.045, compared to 0.22 ± 0.053 in individuals above the median age. By regression analysis, older age was associated with decreased OEF in the whole brain ($p = 0.014$) and cortical gray matter (0.021), but not the white matter (0.12), even after excluding WMH ($p = 0.13$).

By region, older age was associated with decreased OEF in the frontal lobe gyri ($p = 0.017–0.046$), superior parietal lobules ($p = 0.012$), posterior/isthmus cingulate ($p = 0.035$, 0.025), precuneus ($p = 0.031$), supramarginal gyri ($p = 0.025$), inferior temporal gyri ($p = 0.012$), and fusiform gyri ($p = 0.039$) (Figures 1 and 2), but not deep gray nuclei ($p > 0.05$). After correction with multiple comparisons, there was only a trend for decreased OEF in the superior frontal gyri, hippocampi, and fusiform gyri (adjusted $p = 0.08$, 0.09, 0.09, respectively).

In the cognitively impaired cohort, individuals below the median age had a mean whole brain OEF of 0.24 ± 0.047, compared to 0.22 ± 0.042 in individuals above the median age. By regression analysis, age was not associated with OEF in the whole brain ($p = 0.07$), cortical gray matter ($p = 0.26$), or white matter ($p = 0.17$). Similarly, age was not associated with OEF in most frontal, parietal, and temporal lobe regions ($p > 0.05$). However, older age

was associated with decreased OEF in the hippocampus (p = 0.027) and caudate (p = 0.014), although adjusted p-values after correction for multiple comparisons were not significant (adjusted p = 0.31, 0.32, respectively).

White matter hyperintensity burden showed associations with oxygen extraction in the cognitively impaired group

In the cognitively intact group, individuals with a WMH burden below the median had a mean whole brain OEF of 0.25 ± 0.054, compared to 0.23 ± 0.049 in individuals with a WMH burden above the median. WMH burden was not associated with OEF in the whole brain (p = 0.43), cortical gray matter (p = 0.67), white matter (p = 0.41), or any brain region (Figures 1 and 2).

In the cognitively impaired cohort, individuals with a WMH burden below the median had a mean whole brain OEF of 0.24 ± 0.046, compared to 0.22 ± 0.043 in individuals with a WMH burden above the median. Increasing WMH burden was associated with decreased OEF in the white matter (p = 0.026), but not in the whole brain (p = 0.06) or in cortical gray matter (p = 0.14). By region, increasing WMH burden was associated with decreased OEF in the hippocampus (p = 0.011), superior temporal gyri (p = 0.026), and caudate nuclei (p < 0.001). The association between WMH burden and OEF in the caudate persisted after adjustment for multiple comparisons (adjusted p = 0.0026). There were no associations between WMH and OEF in other brain regions (p > 0.05).

Age and white matter hyperintensity burden showed mild regional associations with tissue susceptibility in temporoparietal regions in the cognitively impaired

Associations between age and WMH burden and regional tissue susceptibility, as measured by χ_n, are shown in Figure 3.

In the cognitively impaired, individuals below the median age had a cortical gray matter χ_n of −9.47 ± 5.47, compared to −7.79 ± 5.35 ppb for individuals above the median age. There was no association between increasing age or WMH burden and χ_n in the cortical gray matter (p = 0.11, 0.33, respectively).

By region, increasing age was associated with higher χ_n in the posterior/isthmus cingulate (p = 0.028, p=0.001), superior temporal gyri (p = 0.011), inferior temporal gyri (p = 0.017), putamen (p = 0.009), and pallidum (p = 0.032). The association between age and χ_n in the isthmus cingulate persisted after adjusting for multiple comparisons (adjusted p = 0.02), whereas trends were seen between age and superior temporal gyri, putamen, and inferior temporal gyri (adjusted p = 0.07, 0.09, 0.09, respectively).

Individuals with a WMH burden below the median had a χ_n of −9.76 ± 5.26, compared to −8.30 ± 5.92 for individuals with a WMH above the median. Increasing WMH burden was associated with higher brain iron levels in the isthmus cingulate (p = 0.006), superior/middle/inferior temporal gyri (p = 0.029, 0.007, 0.025), and the caudate nuclei (p = 0.004). The association between WMH burden and χ_n of the middle temporal gyri persisted after adjustment for multiple comparisons (adjusted p = 0.047), whereas trends were seen

between WMH burden and χ_n of the isthmus cingulate and caudate (adjusted p = 0.06, 0.08).

In the cognitively intact cohort, there were no significant associations between age or WMH burden and tissue susceptibility (p > 0.05). Individuals below the median age had a χ_n of −12.79 ± 8.27, compared to −14.41 ± 7.19 for individuals above the median age. Individuals with a WMH burden below the median had a χ_n of −13.01 ± 8.39, compared to −14.19 ± 7.10 for individuals with a WMH above the median.

Cognitively impaired subjects had higher regional tissue susceptibility and higher oxygen extraction than cognitively intact subjects

In multivariate regression analyses, adjusting for age and WMH, cognitive impairment was associated with higher OEF in the cortical gray matter (p < 0.001), but was not associated with OEF in the whole brain (p = 0.97) or white matter (p = 0.61). Cognitive impairment was also associated with higher OEF in the frontal lobe gyri (p < 0.001), superior and inferior parietal lobules (p < 0.001), posterior cingulate/precuneus (p < 0.001), isthmus cingulate (p = 0.01), and superior (p < 0.001) and middle temporal lobe gyri (p = 0.048) (Figure 4). After adjustment for multiple comparisons, associations between cognitive impairment and OEF persisted in the frontal lobe gyri (adjusted p < 0.001), parietal lobe regions including the posterior cingulate and precuneus (adjusted p < 0.001), isthmus cingulate (adjusted p = 0.02), and superior temporal gyri (p < 0.001).

Cognitive impairment was associated with higher χ_n in the cortical gray matter (p = 0.005), adjusted for age and WMH burden. Cognitive impairment was associated with higher tissue susceptibility in frontal lobe gyri (ranging from p < 0.001 to 0.017), superior and inferior parietal lobules (p < 0.001), supramarginal gyri (p = 0.01), precuneus (p = 0.009), superior temporal lobe gyri (p = 0.037), pallidum (p = 0.002) and putamen (p = 0.027). After adjustment for multiple comparisons, associations between cognitive impairment and χ_n persisted in the frontal lobe gyri (adjusted p ranging from < 0.001 to 0.038), parietal lobe regions (adjusted p ranging from < 0.001 to 0.03), and pallidum (p = 0.007).

Discussion:

Our study investigated the effects of age and WMH burden on brain OEF and tissue susceptibility in cognitively impaired and cognitively intact clinical patients. Our first major finding was that age showed associations with OEF in the cognitively intact patients, whereas WMH burden showed associations with OEF in the cognitively impaired patients. Secondly, we found that both age and WMH burden showed regional associations with brain χ_n in the cognitively impaired patients, but not in the cognitively intact. Finally, we found that cognitively impaired patients had higher OEF and brain χ_n compared to the cognitively intact subjects.

The first major finding was that older age showed associations with decreased OEF in the cognitively intact rather than impaired group. Older age is known to be a strong predictor of dementia[34] and the pathological hallmark of disease, beta-amyloid plaques, also increases in parallel with age.[55] One can consider OEF a measure of metabolic function in the brain,

since extraction and utilization of oxygen is required for aerobic metabolism. Thus, either due to the presence of increasing beta-amyloid or other cellular and environmental stresses related to aging, it is not surprising that neuronal function, as assessed by OEF, would decrease with older age. This is compatible with prior articles that used PET and reported decreased OEF in neocortical areas with increasing age.[56,57] However, this differs from an MR study that measured global rather than regional OEF using the superior sagittal sinus[58] and another study that found no significant association between age and OEF.[59] These inconsistent findings may be due to differences in technique, since regional decreases are suppressed in global measurements, and differences in cohort selection, such as including subjects much younger than 50 years of age. Of note, cerebral blood flow is known to decrease with age.[60] However, in a setting of low cerebral perfusion, OEF typically increases as a compensatory measure to maintain cerebral metabolism,[61] so we do not believe the observed OEF decrease is related to decreased cerebral blood flow. Interestingly, age was not significantly associated with OEF in our cognitively impaired group in most brain regions. It is possible that once cognitive impairment is present, age-related effects are overshadowed by disease-related effects on brain oxygen utilization, such as detrimental effects from beta-amyloid plaques and phosphorylated tau on mitochondria.[62,63] Notably, older age was associated with decreased OEF in the hippocampus, even in cognitively impaired subjects, which suggests that age-related changes continue to have detrimental effects on the hippocampus, which is known to show accelerated atrophy with ongoing cognitive impairment.[64]

The second major finding was that, unlike age, WMH showed associations with OEF in the cognitively impaired group. A prior pathological study reported that WMH are associated with vascular pathology in cognitively normal individuals, whereas WMH are associated with AD pathology in cognitively impaired individuals.[65] It is likely that, our cognitively intact group did not have severe enough vascular disease to cause changes in the OEF, in the absence of AD pathology. On the other hand, the cognitively impaired group likely already had underlying AD pathology, and superimposed vascular disease could have contributed to the decline in OEF in already irreversibly damaged brain tissue. This finding thus lends credence to the idea of a two-hit hypothesis of AD, such that vascular disease combines with preexisting AD pathology to cause a significant decline in OEF,[66] rather than either process alone. Also of note, whole white matter OEF decreased with increasing WMH burden, which is compatible with a prior study reporting decreased tissue oxygenation in WMH.[67]

The third major finding was that both age and WMH burden showed mild regional associations with χ_n in the cognitively impaired, but not in the cognitively intact group. Although a prior study reported an association between increasing age and iron levels, particularly in motor and premotor areas,[68] we did not find this association in our cognitively intact group. Our χ_n parameter is believed to measure tissue contribution to total susceptibility within a voxel that is not in a blood vessel, just as a vein. In our cognitively impaired group, this tissue susceptibility could result from iron deposition, possibly accompanying AD pathology,[3–5,51,69,70] or myelin breakdown and loss, due to aging and/or neurodegeneration.[71–73] The association between WMH burden and χ_n in the cognitively impaired is also consistent with prior literature suggesting that WMH are associated with beta-amyloid plaques in AD, since iron can be found in amyloid plaques and

contribute to tissue susceptibility.[65] Another study suggested an inverse relationship between cerebral blood flow and brain iron deposition,[74] possibly due to myelin breakdown and loss in the face of declining cerebral blood flow, leading to release of iron by degenerating oligodendrocytes and myelin.[71–73]

Finally, we found that cognitively impaired subjects had higher regional χ_n and higher OEF than cognitively intact subjects, adjusted for age and WMH burden. The finding of higher χ_n in the cognitively impaired is consistent with prior literature demonstrating increased iron among individuals with AD.[4,5,75,76] Both pathological and imaging studies have demonstrated that iron colocalizes with beta-amyloid plaques.[9–13,69,77] Although amyloid PET was not performed on our clinical cohort, it is highly likely that many of these cognitively impaired patients had brain amyloidosis, which could in turn explain higher levels of brain iron. In addition, myelin breakdown has been implicated in AD and other neurodegenerative disorders[72] and could also contribute to release of iron, increasing χ_n. The finding of elevated OEF in the cognitively impaired patients was surprising. Prior studies investigating OEF in AD have been conflicting, with some showing increased OEF in the temporal and parietal cortices,[78–80] as well as the white matter,[79] whereas others have reported decreased OEF.[81–83] The conflicting findings in the literature may reflect early versus late changes in AD. Some have postulated that decreased cerebral blood flow from capillary dysfunction could lead to an early compensatory rise in OEF,[58,84,85] similar to the increased OEF reported with atherosclerotic stenoses.[86] A similar compensatory increase in metabolism, as seen on FDG-PET, has also been reported at early stages of AD.[87–91] Since our cohort of cognitively impaired patients were undergoing MRI primarily to exclude other causes of dementia, they were likely early in their disease course. As AD progresses, it is likely that OEF will decrease, as neuronal dysfunction leads to impaired oxygen metabolism.

Our study had several limitations. First, this was a clinical cohort, so deep phenotyping with amyloid or tau PET was not available. As a result, we can only surmise the changes in iron and OEF are related to underlying AD pathology, but confirming this in larger cohorts will be a focus of future work. Secondly, QSM maps can show susceptibility artifacts along the calvarium, including the skull base, but we tried to mitigate these artifacts by excluded voxels within 5 mm of the outside boundary of the brain in our standard processing pipeline. Finally, our cognitively normal cohort was a convenience sample, established via detailed chart review and imaging. However, they did not undergo extensive neuropsychological testing to prove normal cognitive function. Nevertheless, we believe that our study provides evidence for using both QSM and OEF to better understand pathophysiological changes relative to aging, WMH, and cognitive impairment and demonstrates feasibility in clinical practice.

In conclusion, higher brain OEF and iron in cognitively impaired older individuals may reflect altered oxygen metabolism due to underlying AD pathology, particularly amyloid, which is known to colocalize with iron in the brain. Both age and WMH have associations with brain iron and oxygen extraction, but are modulated by the presence of cognitive impairment.

Acknowledgements and Disclosures:

JC and YW are inventors of QSM-related patents issued to/applied for by Cornell University. YW owns equity in Medimagemetric LLC.

Funding:

Research reported in this publication was supported in part by the following grants: National Institutes of Health/National Institute on Aging R01AG068398 (G.C.), National Institutes of Health/National Institute of Neurological Disorders and Stroke K99 NS123229 (J.C.), National Institutes of Health/National Institute on Aging R21 AG067466 (I.K., Y.W.), National Institutes of Health/National Institute of Neurological Disorders and Stroke R01 NS095562 (Y.W.), National Institutes of Health/National Institute on Aging RF1AG057570 (M.D.) grants. This project was supported in part by funds from the Clinical Translational Science Center (CTSC), National Center for Advancing Translational Sciences (NCATS) grant number UL1-RR024996.

References:

1. Hale JM, Schneider DC, Gampe J, Mehta NK, Myrskyla M. Trends in the risk of cognitive impairment in the United States, 1996–2014. Epidemiology 2020;31:745–54. [PubMed: 32740472]
2. Clarfield AM. The decreasing prevalence of reversible dementias: an updated meta-analysis. Arch Intern Med 2003;163:2219–29. [PubMed: 14557220]
3. Ayton S, Fazlollahi A, Bourgeat P, et al. Cerebral quantitative susceptibility mapping predicts amyloid-beta-related cognitive decline. Brain 2017;140:2112–9. [PubMed: 28899019]
4. Kim HG, Park S, Rhee HY, et al. Quantitative susceptibility mapping to evaluate the early stage of Alzheimer's disease. Neuroimage Clin 2017;16:429–38. [PubMed: 28879084]
5. Du L, Zhao Z, Cui A, et al. Increased iron deposition on brain quantitative susceptibility mapping correlates with decreased cognitive function in Alzheimer's disease. ACS Chem Neurosci 2018;9:1849–57. [PubMed: 29722955]
6. Moon Y, Han SH, Moon WJ. Patterns of brain iron accumulation in vascular dementia and Alzheimer's dementia using quantitative susceptibility mapping imaging. J Alzheimers Dis 2016;51:737–45. [PubMed: 26890777]
7. Acosta-Cabronero J, Williams GB, Cardenas-Blanco A, Arnold RJ, Lupson V, Nestor PJ. In vivo quantitative susceptibility mapping (QSM) in Alzheimer's disease. PLoS One 2013;8:e81093. [PubMed: 24278382]
8. van Bergen JM, Li X, Hua J, et al. Colocalization of cerebral iron with amyloid beta in mild cognitive impairment. Sci Rep 2016;6:35514. [PubMed: 27748454]
9. Smith MA, Harris PL, Sayre LM, Perry G. Iron accumulation in Alzheimer disease is a source of redox-generated free radicals. Proc Natl Acad Sci U S A 1997;94:9866–8. [PubMed: 9275217]
10. Smith MA, Zhu X, Tabaton M, et al. Increased iron and free radical generation in preclinical Alzheimer disease and mild cognitive impairment. J Alzheimers Dis 2010;19:363–72. [PubMed: 20061651]
11. van Duijn S, Bulk M, van Duinen SG, et al. Cortical iron reflects severity of Alzheimer's disease. J Alzheimers Dis 2017;60:1533–45. [PubMed: 29081415]
12. Zeineh MM, Chen Y, Kitzler HH, Hammond R, Vogel H, Rutt BK. Activated iron-containing microglia in the human hippocampus identified by magnetic resonance imaging in Alzheimer disease. Neurobiol Aging 2015;36:2483–500. [PubMed: 26190634]
13. Gallagher JJ, Finnegan ME, Grehan B, Dobson J, Collingwood JF, Lynch MA. Modest amyloid deposition is associated with iron dysregulation, microglial activation, and oxidative stress. J Alzheimers Dis 2012;28:147–61. [PubMed: 21971404]
14. de Rochefort L, Liu T, Kressler B, et al. Quantitative susceptibility map reconstruction from MR phase data using bayesian regularization: validation and application to brain imaging. Magn Reson Med 2010;63:194–206. [PubMed: 19953507]
15. Liu T, Spincemaille P, de Rochefort L, Wong R, Prince M, Wang Y. Unambiguous identification of superparamagnetic iron oxide particles through quantitative susceptibility mapping of the nonlinear response to magnetic fields. Magn Reson Imaging 2010;28:1383–9. [PubMed: 20688448]

16. Bilgic B, Pfefferbaum A, Rohlfing T, Sullivan EV, Adalsteinsson E. MRI estimates of brain iron concentration in normal aging using quantitative susceptibility mapping. Neuroimage 2012;59:2625–35. [PubMed: 21925274]
17. Langkammer C, Schweser F, Krebs N, et al. Quantitative susceptibility mapping (QSM) as a means to measure brain iron? A post mortem validation study. Neuroimage 2012;62:1593–9. [PubMed: 22634862]
18. Wang Y, Liu T. Quantitative susceptibility mapping (QSM): Decoding MRI data for a tissue magnetic biomarker. Magn Reson Med 2015;73:82–101. [PubMed: 25044035]
19. Zhang Y, Gauthier SA, Gupta A, et al. Longitudinal change in magnetic susceptibility of new enhanced multiple sclerosis (MS) lesions measured on serial quantitative susceptibility mapping (QSM). J Magn Reson Imaging 2016;44:426–32. [PubMed: 26800367]
20. Langkammer C, Krebs N, Goessler W, et al. Quantitative MR imaging of brain iron: a postmortem validation study. Radiology 2010;257:455–62. [PubMed: 20843991]
21. Gillen KM, Mubarak M, Park C, et al. QSM is an imaging biomarker for chronic glial activation in multiple sclerosis lesions. Ann Clin Transl Neurol 2021;8:877–86. [PubMed: 33704933]
22. Spincemaille P, Liu Z, Zhang S, et al. Clinical integration of automated processing for brain quantitative susceptibility mapping: Multi-site reproducibility and single-site robustness. J Neuroimaging 2019;29:689–98. [PubMed: 31379055]
23. Deh K, Nguyen TD, Eskreis-Winkler S, et al. Reproducibility of quantitative susceptibility mapping in the brain at two field strengths from two vendors. J Magn Reson Imaging 2015;42:1592–600. [PubMed: 25960320]
24. Cho J, Kee Y, Spincemaille P, et al. Cerebral metabolic rate of oxygen (CMRO2) mapping by combining quantitative susceptibility mapping (QSM) and quantitative blood oxygenation level-dependent imaging (qBOLD). Magn Reson Med 2018;80:1595–604. [PubMed: 29516537]
25. Cho J, Zhang S, Kee Y, et al. Cluster analysis of time evolution (CAT) for quantitative susceptibility mapping (QSM) and quantitative blood oxygen level-dependent magnitude (qBOLD)-based oxygen extraction fraction (OEF) and cerebral metabolic rate of oxygen (CMRO2) mapping. Magn Reson Med 2020;83:844–57. [PubMed: 31502723]
26. Cho J, Spincemaille P, Nguyen TD, Gupta A, Wang Y. Temporal clustering, tissue composition, and total variation for mapping oxygen extraction fraction using QSM and quantitative BOLD. Magn Reson Med 2021;86:2635–46. [PubMed: 34110656]
27. Cho J, Lee J, An H, Goyal MS, Su Y, Wang Y. Cerebral oxygen extraction fraction (OEF): Comparison of challenge-free gradient echo QSM+qBOLD (QQ) with (15)O PET in healthy adults. J Cereb Blood Flow Metab 2021;41:1658–68. [PubMed: 33243071]
28. Cho J, Zhang J, Spincemaille P, et al. QQ-NET - using deep learning to solve quantitative susceptibility mapping and quantitative blood oxygen level dependent magnitude (QSM+qBOLD or QQ) based oxygen extraction fraction (OEF) mapping. Magn Reson Med 2021;87:1583–94 [PubMed: 34719059]
29. Kudo K, Liu T, Murakami T, et al. Oxygen extraction fraction measurement using quantitative susceptibility mapping: Comparison with positron emission tomography. J Cereb Blood Flow Metab 2016;36:1424–33. [PubMed: 26661168]
30. Wu D, Zhou Y, Cho J, et al. The spatiotemporal evolution of MRI-derived oxygen extraction fraction and perfusion in ischemic stroke. Front Neurosci 2021;15:716031. [PubMed: 34483830]
31. Zhang S, Cho J, Nguyen TD, et al. Initial experience of challenge-free MRI-based oxygen extraction fraction mapping of ischemic stroke at various stages: Comparison with perfusion and diffusion mapping. Front Neurosci 2020;14:535441. [PubMed: 33041755]
32. Cho J, Nguyen TD, Huang W, et al. Brain oxygen extraction fraction mapping in patients with multiple sclerosis. J Cereb Blood Flow Metab 2022;42:338–48 [PubMed: 34558996]
33. Prins ND, van Dijk EJ, den Heijer T, et al. Cerebral white matter lesions and the risk of dementia. Arch Neurol 2004;61:1531–4. [PubMed: 15477506]
34. van der Flier WM, Scheltens P. Epidemiology and risk factors of dementia. J Neurol Neurosurg Psychiatry 2005;76 Suppl 5:v2–7. [PubMed: 16291918]

35. Nasreddine ZS, Phillips NA, Bedirian V, et al. The Montreal Cognitive Assessment, MoCA: a brief screening tool for mild cognitive impairment. J Am Geriatr Soc 2005;53:695–9. [PubMed: 15817019]
36. Folstein MF, Folstein SE, McHugh PR. “Mini-mental state”. A practical method for grading the cognitive state of patients for the clinician. J Psychiatr Res 1975;12:189–98. [PubMed: 1202204]
37. Kokmen E, Smith GE, Petersen RC, Tangalos E, Ivnik RC. The short test of mental status. Correlations with standardized psychometric testing. Arch Neurol 1991;48:725–28. [PubMed: 1859300]
38. Liu T, Wisnieff C, Lou M, Chen W, Spincemaille P, Wang Y. Nonlinear formulation of the magnetic field to source relationship for robust quantitative susceptibility mapping. Magn Reson Med 2013;69:467–76. [PubMed: 22488774]
39. Liu T, Khalidov I, de Rochefort L, et al. A novel background field removal method for MRI using projection onto dipole fields (PDF). NMR Biomed 2011;24:1129–36. [PubMed: 21387445]
40. Liu J, Liu T, de Rochefort L, et al. Morphology enabled dipole inversion for quantitative susceptibility mapping using structural consistency between the magnitude image and the susceptibility map. Neuroimage 2012;59:2560–8. [PubMed: 21925276]
41. Liu Z, Spincemaille P, Yao Y, Zhang Y, Wang Y. MEDI+0: Morphology enabled dipole inversion with automatic uniform cerebrospinal fluid zero reference for quantitative susceptibility mapping. Magn Reson Med 2018;79:2795–803. [PubMed: 29023982]
42. Zhang J, Cho J, Zhou D, et al. Quantitative susceptibility mapping-based cerebral metabolic rate of oxygen mapping with minimum local variance. Magn Reson Med 2018;79:172–9. [PubMed: 28295523]
43. Zhang J, Zhou D, Nguyen TD, Spincemaille P, Gupta A, Wang Y. Cerebral metabolic rate of oxygen (CMRO2) mapping with hyperventilation challenge using quantitative susceptibility mapping (QSM). Magn Reson Med 2017;77:1762–73. [PubMed: 27120518]
44. Zhang J, Liu T, Gupta A, Spincemaille P, Nguyen TD, Wang Y. Quantitative mapping of cerebral metabolic rate of oxygen (CMRO2) using quantitative susceptibility mapping (QSM). Magn Reson Med 2015;74:945–52. [PubMed: 25263499]
45. Ulrich X, Yablonskiy DA. Separation of cellular and BOLD contributions to T2* signal relaxation. Magn Reson Med 2016;75:606–15. [PubMed: 25754288]
46. He X, Zhu M, Yablonskiy DA. Validation of oxygen extraction fraction measurement by qBOLD technique. Magn Reson Med 2008;60:882–8. [PubMed: 18816808]
47. Yablonskiy DA, Sukstanskii AL, He X. Blood oxygenation level-dependent (BOLD)-based techniques for the quantification of brain hemodynamic and metabolic properties - theoretical models and experimental approaches. NMR Biomed 2013;26:963–86. [PubMed: 22927123]
48. Zhang Y, Brady M, Smith S. Segmentation of brain MR images through a hidden Markov random field model and the expectation-maximization algorithm. IEEE Trans Med Imaging 2001;20:45–57. [PubMed: 11293691]
49. Fischl B, Salat DH, Busa E, et al. Whole brain segmentation: automated labeling of neuroanatomical structures in the human brain. Neuron 2002;33:341–55. [PubMed: 11832223]
50. Chiang GC, Insel PS, Tosun D, et al. Identifying cognitively healthy elderly individuals with subsequent memory decline by using automated MR temporoparietal volumes. Radiology 2011;259:844–51. [PubMed: 21467255]
51. van Bergen JMG, Li X, Quevenco FC, et al. Simultaneous quantitative susceptibility mapping and Flutemetamol-PET suggests local correlation of iron and beta-amyloid as an indicator of cognitive performance at high age. Neuroimage 2018;174:308–16. [PubMed: 29548847]
52. Schwarz CG, Gunter JL, Wiste HJ, et al. A large-scale comparison of cortical thickness and volume methods for measuring Alzheimer’s disease severity. Neuroimage Clin 2016;11:802–12. [PubMed: 28050342]
53. Zhang H, Zhang J, Wang R, Zhang Q, Spincemaille P, Nguyen TD, Wang Y. Efficient folded attention for medical image reconstruction and segmentation. Proc AAAI Conf Artif Intell 2021;35:10868–76.
54. Benjamini YHY. Controlling the false discovery rate - a practical and powerful approach to multiple testing. J R Stat Soc B 1995;57:289–300.

55. Jansen WJ, Ossenkoppele R, Knol DL, et al. Prevalence of cerebral amyloid pathology in persons without dementia: a meta-analysis. JAMA 2015;313:1924–38. [PubMed: 25988462]
56. Eustache F, Rioux P, Desgranges B, et al. Healthy aging, memory subsystems and regional cerebral oxygen consumption. Neuropsychologia 1995;33:867–87. [PubMed: 7477814]
57. Yamaguchi T, Kanno I, Uemura K, et al. Reduction in regional cerebral metabolic rate of oxygen during human aging. Stroke 1986;17:1220–8. [PubMed: 3492786]
58. Peng SL, Dumas JA, Park DC, et al. Age-related increase of resting metabolic rate in the human brain. Neuroimage 2014;98:176–83. [PubMed: 24814209]
59. Marchal G, Rioux P, Petit-Taboue MC, et al. Regional cerebral oxygen consumption, blood flow, and blood volume in healthy human aging. Arch Neurol 1992;49:1013–20. [PubMed: 1417508]
60. Pantano P, Baron JC, Lebrun-Grandie P, Duquesnoy N, Bousser MG, Comar D. Regional cerebral blood flow and oxygen consumption in human aging. Stroke 1984;15:635–41. [PubMed: 6611613]
61. Fan AP, An H, Moradi F, et al. Quantification of brain oxygen extraction and metabolism with [(15)O]-gas PET: A technical review in the era of PET/MRI. Neuroimage 2020;220:117136. [PubMed: 32634594]
62. Chen JX, Yan SD. Amyloid-beta-induced mitochondrial dysfunction. J Alzheimers Dis 2007;12:177–84. [PubMed: 17917162]
63. Kandimalla R, Manczak M, Fry D, Suneetha Y, Sesaki H, Reddy PH. Reduced dynamin-related protein 1 protects against phosphorylated Tau-induced mitochondrial dysfunction and synaptic damage in Alzheimer's disease. Hum Mol Genet 2016;25:4881–97. [PubMed: 28173111]
64. Jack CR Jr., Shiung MM, Gunter JL, et al. Comparison of different MRI brain atrophy rate measures with clinical disease progression in AD. Neurology 2004;62:591–600. [PubMed: 14981176]
65. Arfanakis K, Evia AM, Leurgans SE, et al. Neuropathologic correlates of white matter hyperintensities in a community-based cohort of older adults. J Alzheimers Dis 2020;73:333–45. [PubMed: 31771057]
66. Provenzano FA, Muraskin J, Tosto G, et al. White matter hyperintensities and cerebral amyloidosis: necessary and sufficient for clinical expression of Alzheimer disease? JAMA Neurol 2013;70:455–61. [PubMed: 23420027]
67. Dalby RB, Eskildsen SF, Videbech P, et al. Oxygenation differs among white matter hyperintensities, intersected fiber tracts and unaffected white matter. Brain Commun 2019;1:fcz033. [PubMed: 32954272]
68. Acosta-Cabronero J, Betts MJ, Cardenas-Blanco A, Yang S, Nestor PJ. In Vivo MRI Mapping of Brain Iron Deposition across the Adult Lifespan. J Neurosci 2016;36:364–74. [PubMed: 26758829]
69. Tiepolt S, Schafer A, Rullmann M, et al. Quantitative susceptibility mapping of amyloid-beta aggregates in Alzheimer's disease with 7T MR. J Alzheimers Dis 2018;64:393–404. [PubMed: 29865069]
70. Bartzokis G, Tishler TA. MRI evaluation of basal ganglia ferritin iron and neurotoxicity in Alzheimer's and Huntingon's disease. Cell Mol Biol (Noisy-le-grand) 2000;46:821–33. [PubMed: 10875443]
71. Khattar N, Triebswetter C, Kiely M, et al. Investigation of the association between cerebral iron content and myelin content in normative aging using quantitative magnetic resonance neuroimaging. Neuroimage 2021;239:118267. [PubMed: 34139358]
72. Bartzokis G, Lu PH, Mintz J. Human brain myelination and amyloid beta deposition in Alzheimer's disease. Alzheimers Dement 2007;3:122–5. [PubMed: 18596894]
73. Bartzokis G, Mintz J, Sultzer D, et al. In vivo MR evaluation of age-related increases in brain iron. AJNR Am J Neuroradiol 1994;15:1129–38. [PubMed: 8073983]
74. Li D, Liu Y, Zeng X, et al. Quantitative study of the changes in cerebral blood flow and iron deposition during progression of Alzheimer's disease. J Alzheimers Dis 2020;78:439–52. [PubMed: 32986675]
75. Tao Y, Wang Y, Rogers JT, Wang F. Perturbed iron distribution in Alzheimer's disease serum, cerebrospinal fluid, and selected brain regions: a systematic review and meta-analysis. J Alzheimers Dis 2014;42:679–90. [PubMed: 24916541]

76. Damulina A, Pirpamer L, Soellradl M, et al. Cross-sectional and longitudinal assessment of brain iron level in Alzheimer disease using 3-T MRI. Radiology 2020:192541.
77. Tuzzi E, Balla DZ, Loureiro JRA, et al. Ultra-high field MRI in Alzheimer's disease: effective transverse relaxation rate and quantitative susceptibility mapping of human brain in vivo and ex vivo compared to histology. J Alzheimers Dis 2020;73:1481–99. [PubMed: 31958079]
78. Nagata K, Sato M, Satoh Y, et al. Hemodynamic aspects of Alzheimer's disease. Ann N Y Acad Sci 2002;977:391–402. [PubMed: 12480778]
79. Tohgi H, Yonezawa H, Takahashi S, et al. Cerebral blood flow and oxygen metabolism in senile dementia of Alzheimer's type and vascular dementia with deep white matter changes. Neuroradiology 1998;40:131–7. [PubMed: 9561514]
80. Yamaji S, Ishii K, Sasaki M, et al. Changes in cerebral blood flow and oxygen metabolism related to magnetic resonance imaging white matter hyperintensities in Alzheimer's disease. J Nucl Med 1997;38:1471–4. [PubMed: 9293811]
81. Thomas BP, Sheng M, Tseng BY, et al. Reduced global brain metabolism but maintained vascular function in amnestic mild cognitive impairment. J Cereb Blood Flow Metab 2017;37:1508–16. [PubMed: 27389176]
82. Jiang D, Lin Z, Liu P, et al. Brain oxygen extraction Is differentially altered by Alzheimer's and vascular diseases. J Magn Reson Imaging 2020;52:1829–37. [PubMed: 32567195]
83. Ishii K, Kitagaki H, Kono M, Mori E. Decreased medial temporal oxygen metabolism in Alzheimer's disease shown by PET. J Nucl Med 1996;37:1159–65. [PubMed: 8965188]
84. Ostergaard L Blood flow, capillary transit times, and tissue oxygenation: the centennial of capillary recruitment. J Appl Physiol (1985) 2020;129:1413–21. [PubMed: 33031017]
85. Nielsen RB, Parbo P, Ismail R, et al. Impaired perfusion and capillary dysfunction in prodromal Alzheimer's disease. Alzheimers Dement (Amst) 2020;12:e12032. [PubMed: 32490139]
86. Liu Z, Li Y. Cortical cerebral blood flow, oxygen extraction fraction, and metabolic rate in patients with middle cerebral artery stenosis or acute stroke. AJNR Am J Neuroradiol 2016;37:607–14. [PubMed: 26680459]
87. Rubinski A, Franzmeier N, Neitzel J, Ewers M, Alzheimer's Disease Neuroimaging I. FDG-PET hypermetabolism is associated with higher tau-PET in mild cognitive impairment at low amyloid-PET levels. Alzheimers Res Ther 2020;12:133. [PubMed: 33076977]
88. Oh H, Habeck C, Madison C, Jagust W. Covarying alterations in Abeta deposition, glucose metabolism, and gray matter volume in cognitively normal elderly. Hum Brain Mapp 2014;35:297–308. [PubMed: 22965806]
89. Merlo S, Spampinato SF, Sortino MA. Early compensatory responses against neuronal injury: A new therapeutic window of opportunity for Alzheimer's disease? CNS Neurosci Ther 2019;25:5–13. [PubMed: 30101571]
90. Ashraf A, Fan Z, Brooks DJ, Edison P. Cortical hypermetabolism in MCI subjects: a compensatory mechanism? Eur J Nucl Med Mol Imaging 2015;42:447–58. [PubMed: 25267349]
91. Willette AA, Modanlo N, Kapogiannis D, Alzheimer's Disease Neuroimaging I. Insulin resistance predicts medial temporal hypermetabolism in mild cognitive impairment conversion to Alzheimer disease. Diabetes 2015;64:1933–40. [PubMed: 25576061]

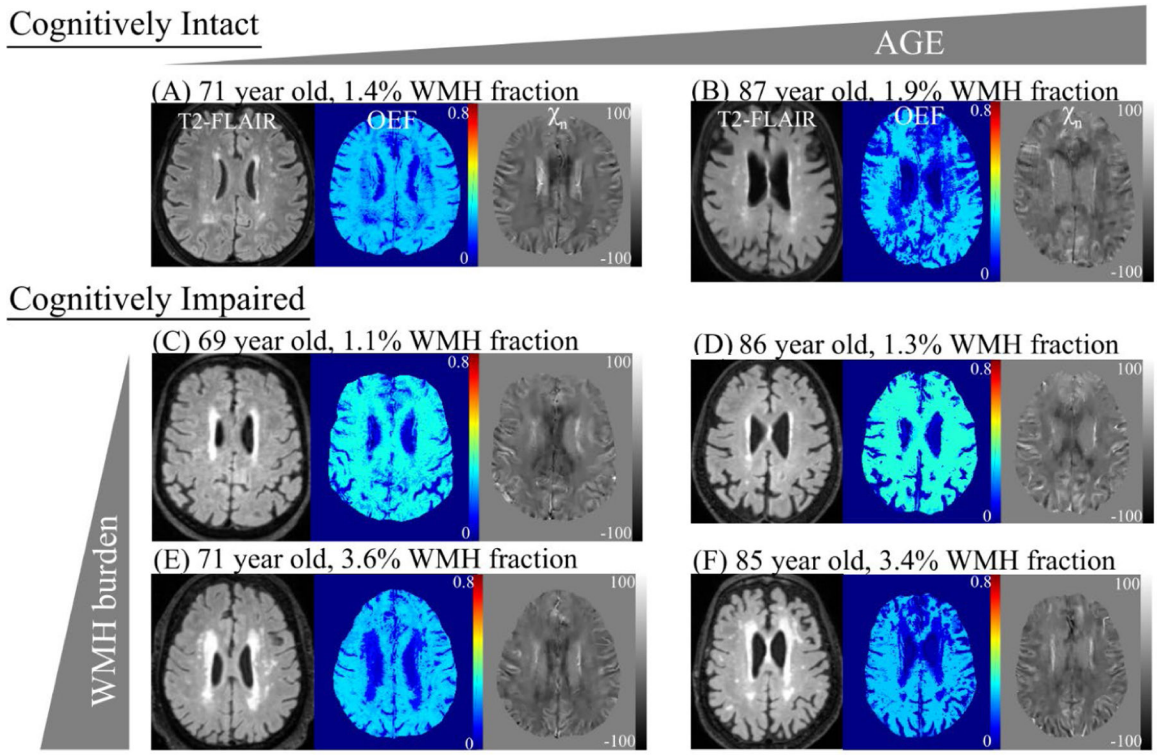

Figure 1.

Oxygen extraction fraction (OEF) and neural tissue susceptibility (χ_n) maps in representative cognitively Intact and impaired subjects. In cognitively intact subjects, OEF decreases with older age (A to B). In cognitively impaired subjects, OEF decreases with increased burden of white matter hyperintensities (WMH), measured as the volume of WMH as a percentage of whole brain volume on a fluid attenuated inversion recovery (FLAIR) sequence (C to E, D to F). Of note, OEF increases with cognitive impairment (A to C, B to D).

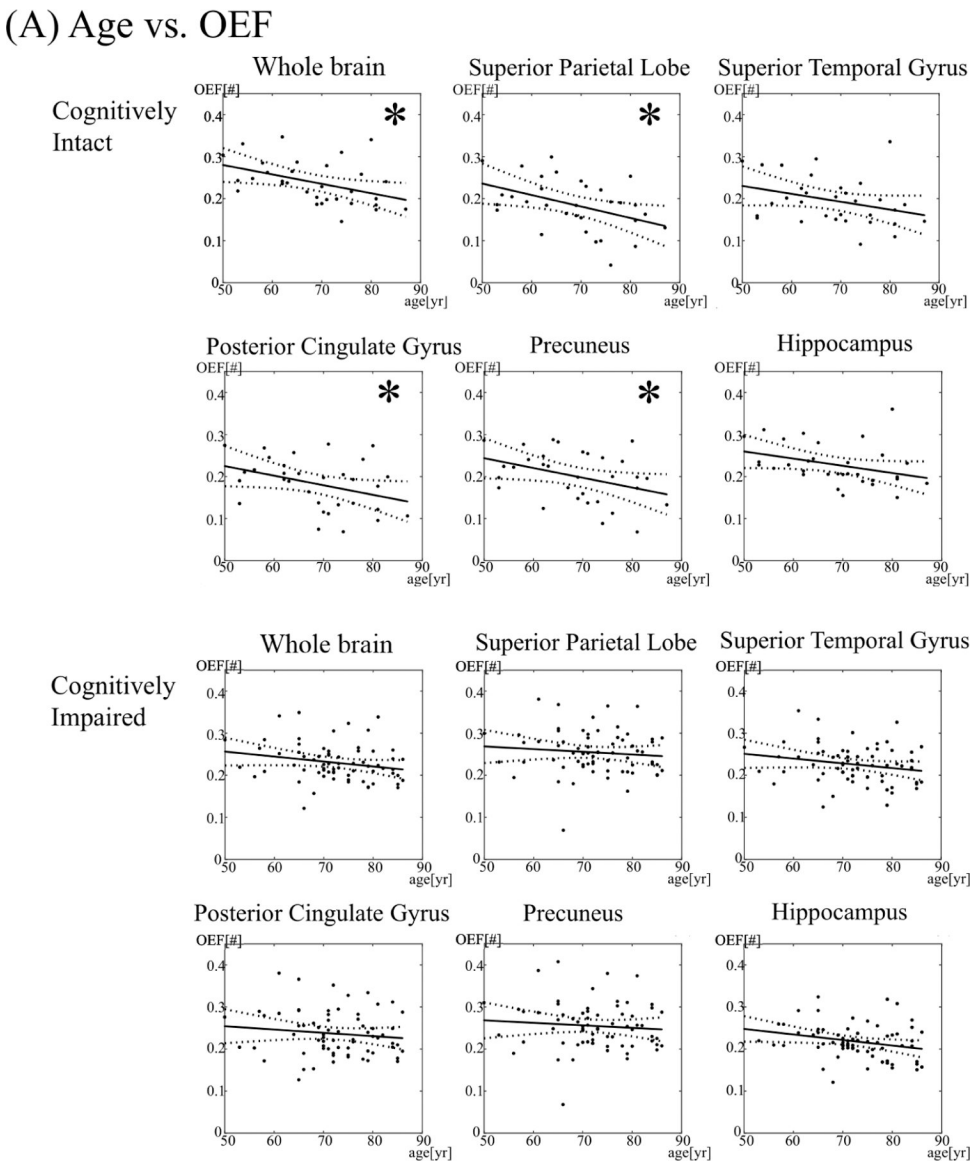

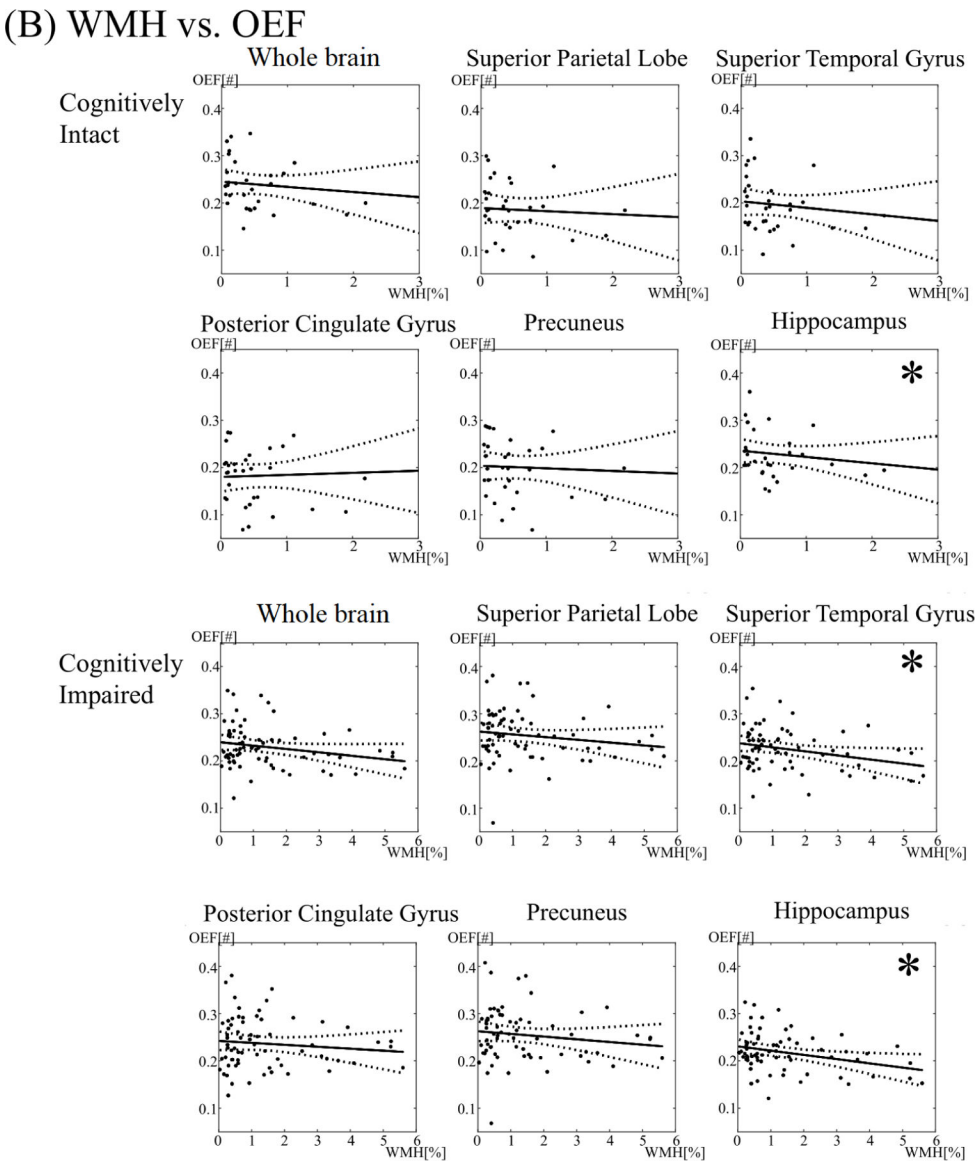

Figure 2. The relationship between oxygen extraction fraction (OEF) and age (A) and white matter hyperintensity (WMH) burden (B) in select brain regions.

The asterisk (*) denotes a significant association ($p < 0.05$). Yr = year.

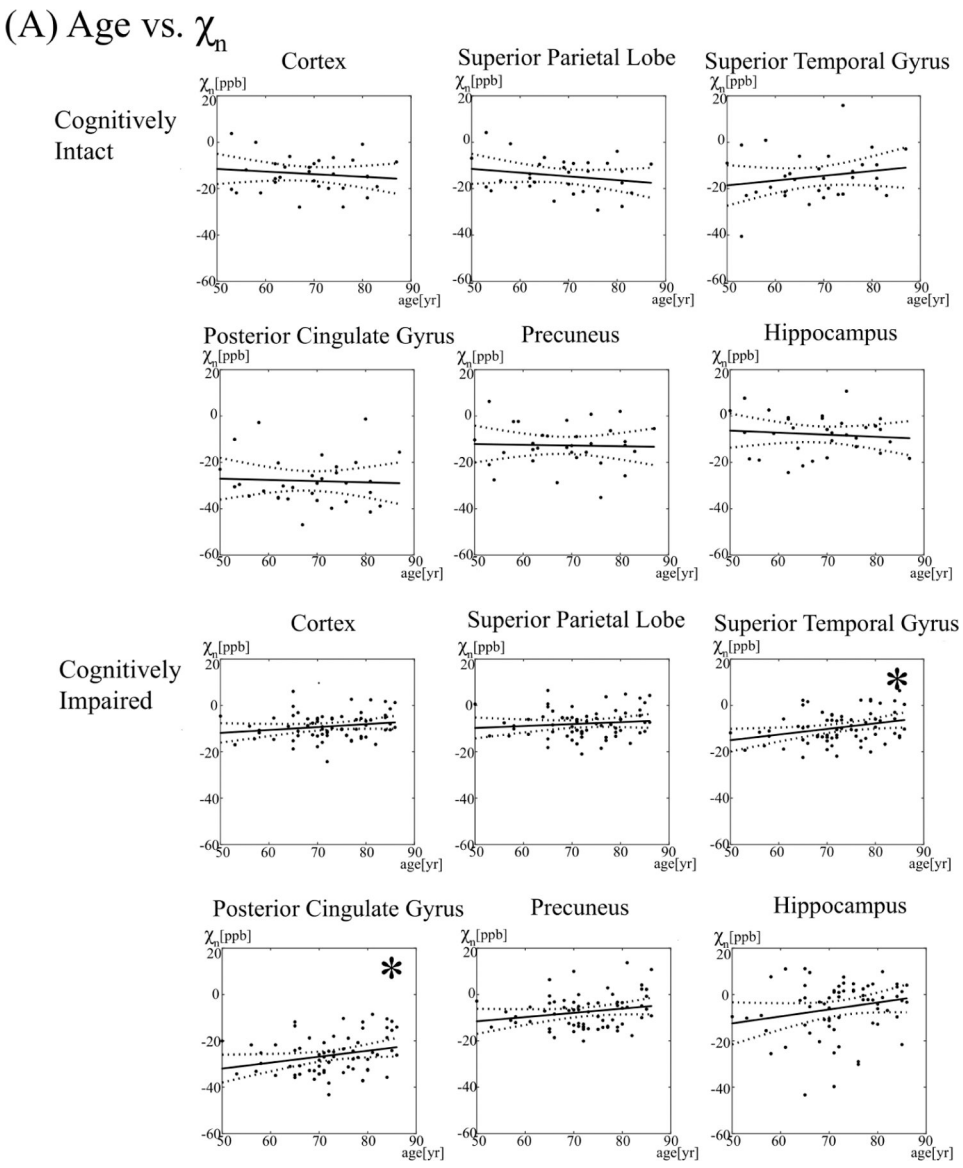

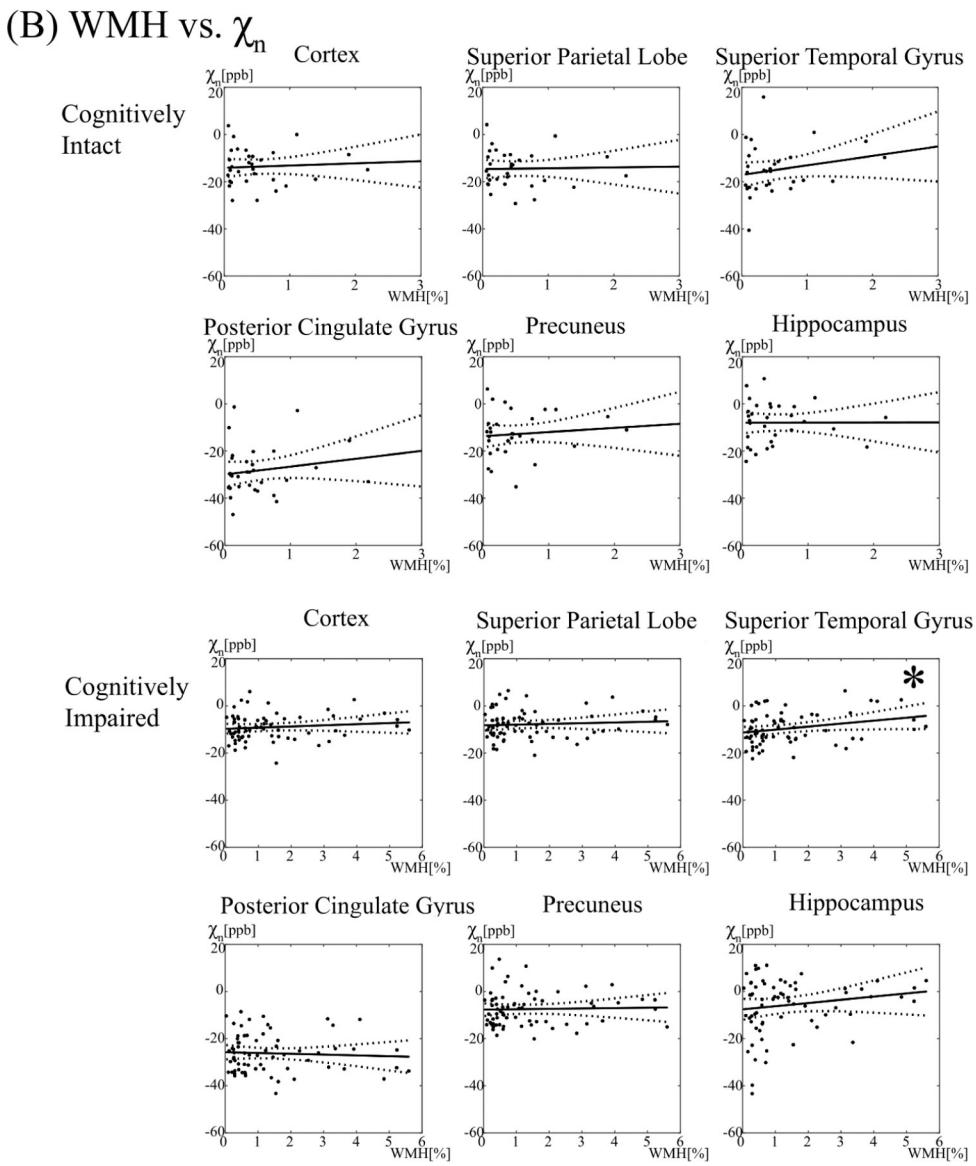

Figure 3. The relationship between neural tissue susceptibility (χ_n) and age (A) and white matter hyperintensity (WMH) burden (B) in select brain regions.

The asterisk (*) denotes a significant association ($p < 0.05$). ppb = parts per billion, yr=year

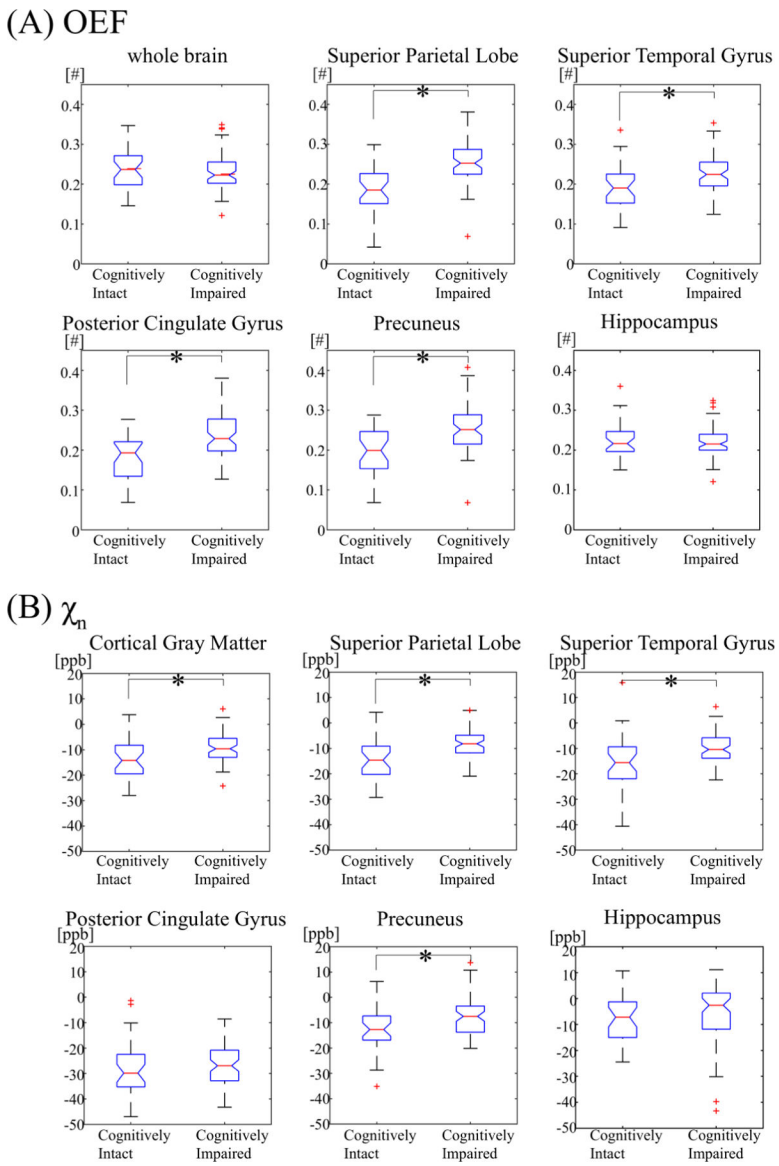

Figure 4. Comparison of oxygen extraction fraction (OEF) (A) and neural tissue susceptibility (χ_n) (B) between cognitively intact and impaired subjects, in select brain regions.

The asterisk (*) denotes a significant association ($p < 0.05$).

Table 1.

Differences in baseline variables between the cognitively impaired and intact groups.

	Cognitively impaired	Cognitively normal	P-value*
Number of patients	68	32	
Age, years	72 (50–86) [8.4]	69 (50–87) [9.9]	0.062
Sex (female:male)	41:27	23:9	0.37
Volume of T2 FLAIR white matter hyperintensities as a percentage of total brain volume, %	1.37 (0.03–5.6) [1.41]	0.58 (0.06–3.1) [0.69]	0.0004*
Whole brain oxygen extraction fraction	0.24 (0.12–0.37) [0.047]	0.25 (0.16–0.37) [0.054]	0.32
Cortical gray matter Neural tissue Susceptibility, in parts per billion	−9.03 (−0.24–6.06) [5.61]	−13.60 (−27.99–3.77) [7.67]	0.0018*

Data shown are means, (range), [standard deviations]

P-value by Wilcoxon rank sum (for continuous variables) and Fisher's exact test (for sex).

* $p < 0.05$

Abbreviation: FLAIR = fluid attenuated inversion recovery